Published in final edited form as:
J Comp Neurol. 2008 August 20; 509(6): 661–676. doi:10.1002/cne.21755.

Espin Actin-Cytoskeletal Proteins Are in Rat Type-I Spiral Ganglion Neurons and Include Splice-Isoforms with a Functional Nuclear Localization Signal

GABRIELLA SEKERKOVÁ, **LILI ZHENG**, **ENRICO MUGNAINI**, and **JAMES R. BARTLES**
Department of Cell & Molecular Biology, Northwestern University Feinberg School of Medicine, Chicago, IL 60611, USA

Abstract

The espins are Ca^{2+}-resistant actin-bundling proteins that are enriched in hair cell stereocilia and sensory cell microvilli. Here, we report a novel localization of espins to a large proportion of rat type-I spiral ganglion neurons (SGNs) and their projections to the cochlear nucleus (CN). Moreover, we show that a fraction of these espins is in the nucleus of SGNs owing to the presence of splice-isoforms that contain a functional nuclear localization signal (NLS). Espin antibody labeled ~83% of type-I SGNs, and the labeling intensity increased dramatically during early postnatal development. Type-II SGNs and vestibular ganglion neurons were unlabeled. In the CN, espin-positive auditory nerve fibers showed a projection pattern typical of type-I SGNs, with intense labeling in the nerve root region and posteroventral CN (PVCN). The anteroventral CN (AVCN) showed moderate labeling, while the dorsal CN showed weak labeling that was restricted to the deep layer. Espin-positive synaptic terminals were enriched around nerve root neurons and octopus cells in the PVCN and were also found on globular bushy cells and multipolar neurons in the PVCN and AVCN. SGNs expressed multiple espin transcripts and proteins, including splice-isoforms that contain a nonapeptide, which is rich in positively charged amino acids and creates a bipartite NLS. The nonapeptide was necessary to target espin isoforms to the nucleus and was sufficient to target an unrelated protein to the nucleus when joined with the upstream di-arginine-containing octapeptide. The presence of cytoplasmic and nuclear espins in SGNs suggest additional roles for espins in auditory neuroscience.

Keywords

auditory nerve; actin-bundling protein; nuclear actin; vomeronasal organ; accessory olfactory bulb; sensory neuron

INTRODUCTION

Spiral ganglion neurons (SGNs) transmit primary acoustic information from cochlear hair cells to the brain. SGNs extend a peripheral process to hair cells and a central process to target neurons in the cochlear nucleus (CN). Two main categories of SGN are commonly recognized: the large, bipolar type-I, which make up ~90–95% of the entire ganglionic population, and the smaller-sized, pseudomonopolar type-II (reviewed in Ryugo and Parks, 2003). Type-I SGNs innervate single inner hair cells, whereas each type-II SGN innervates ~30–60 outer hair cells (Kiang et al., 1982; Hafidi, 1998; Rubel and Fritzsch, 2002). The

Correspondence to: Dr. Gabriella Sekerková, Dept. of Cell and Molecular Biology, Northwestern University Feinberg School of Medicine, 303 East Chicago Avenue, Chicago, IL 60611. Phone: 312-503-4231; FAX: 312-503-7912; E-mail: g-sekerkova@northwestern.edu.

central processes of SGNs bifurcate into ascending and descending branches within the CN and maintain a tonotopic map (Bourk et al., 1981; Ryugo and Parks, 2003). Auditory nerve fibers (ANFs) transmitting low-frequency auditory signals from the apical cochlea arborize in ventral regions of the CN, whereas ANFs transmitting high-frequency auditory signals from the basal cochlea ramify more dorsally. While the central processes of both type-I and type-II SGNs follow this branching organization, they differ in their target cells (Ryugo, 1992; Ryugo and Parks, 2003). Type-I SGNs form their terminals within the magnocellular parts of the CN, the source of ascending projections to the upper auditory brainstem. While the terminal zone of type-II SGNs overlaps that of type-I, type-II SGNs also send collaterals to the surrounding microneuronal shell.

Espins are multifunctional actin-cytoskeletal proteins that are best known for their Ca^{2+}-resistant actin-bundling activity (Bartles et al., 1998; Chen et al., 1999) and ability to elongate parallel actin bundles (PABs) (Loomis et al., 2003). Espins are enriched in the PAB-containing microvillar specializations of mechanosensory or chemosensory cells, such as hair cell stereocilia, and are the target of multiple deafness mutations (Zheng et al., 2000; Naz et al., 2004; Sekerková et al., 2004, 2006b; Donaudy et al., 2006). Espins are also enriched in the actin-rich dendritic spines of cerebellar Purkinje cells (Sekerková et al., 2003) and are distributed diffusely throughout the cytoplasm of epithelial cells undergoing morphogenesis in the developing inner ear, branchial clefts, pharyngeal pouches, lacrimal glands and lungs (Sekerková et al., 2006a). Although espins are encoded by a single gene, differential transcriptional start-site selection and splicing give rise to multiple isoforms that differ significantly in their patterns of expression, ligand-binding sites and biological activities (reviewed in Sekerková et al., 2006b).

In a recent study, we noted that espin isoforms are expressed in complex spatiotemporal patterns during the development of rat inner ear, from otic pit formation through postnatal maturation of the cochlea (Sekerková et al., 2006a). Affinity purified espin antibody specifically labeled neuroblasts within the otocyst, however this labeling was reduced upon neuroblast delamination to form the developing vestibulocochlear ganglion (Sekerková et al., 2006a). This raised the question of whether espin proteins might also be detected in neurons of the spiral ganglion or vestibular ganglion in adults. Here, we report that specific espin isoforms are expressed in a developmentally regulated fashion in a majority of rat type-I SGNs and include splice-isoforms with a functional nuclear localization signal (NLS).

MATERIALS AND METHODS

Animals

Sprague-Dawley rats of either sex (~250 g) and timed-pregnant females were purchased from Harlan (Indianapolis, IN). All experiments conformed to protocols approved by the Northwestern University Animal Care and Use Committee and followed guidelines issued by the National Institutes of Health.

Antibodies

The espin antibody used in this study was raised in a rabbit using a purified recombinant rat espin 2B (formerly called Purkinje cell espin 1; GenBank AA050330) construct as the immunogen and affinity purified on columns of the same rat espin 2B protein covalently coupled to CNBr-activated-Sepharose 4B (Sigma, St. Louis, MO) at 4°C. The rat espin 2B construct was produced in OneShot BL21 (DE3) *E. coli* (Invitrogen, Carlsbad, CA) using the ProEXHTa vector (Invitrogen), which substituted a 26-amino acid N-terminal peptide containing a 6xHis tag and a tobacco etch virus protease cleavage site (MSYYHHHHHHDYDIPTTENLYFQGAM) for the N-terminal 12 amino acids of the 511-

amino acid rat espin 2B protein, and was affinity purified batch-wise using Ni-NTA beads (Qiagen, Valencia, CA) (Chen et al., 1999). Rabbit antiserum (4 ml, pooled bleeds 3–5) was cycled overnight through a 1-ml Sepharose 4B column containing ~8 mg of covalently coupled rat espin 2B construct. After extensive washing with phosphate-buffered saline, the adsorbed antibody was eluted using 0.1 M NaCl, 0.1M glycine-HCl, pH 2.8, and rapidly neutralized by adding 1/4th volume of 0.5M Tris-HCl, pH 8.35, before dialysis against phosphate-buffered saline. This affinity purified espin antibody, which has been used in a number of our previous publications, has been found to react with all known espin isoforms in rats and mice (e.g., Loomis et al., 2003; Sekerková et al., 2003, 2004, 2006a), suggesting that it includes immunoglobulins that bind the C-terminal peptide shared by all espin isoforms (Sekerková et al., 2004). This affinity purified espin antibody has demonstrated its specificity in a variety of contexts. For example, the western blot bands it labels in rat and mouse tissue samples coincide with those observed in transfected tissue culture cells expressing the corresponding espin isoforms exogenously, as well as with those of the bacterially expressed recombinant espin isoform proteins (Loomis et al., 2003; Sekerková et al., 2004). By immunocytochemistry, the espin antibody labels espin-expressing transfected cells, but not untransfected control cells (Serkerková et al., 2004), and there is agreement between the subcellular localizations observed for GFP-tagged espins expressed exogenously in a variety of transfected cell types and the localizations observed upon labeling with the espin antibody, both in the transfected cells and in rat and mouse tissues (Loomis et al., 2003; Sekerková et al., 2004, 2005, 2006a). Whether by western blotting or immunocytochemistry, the espin antibody does not react with specimens prepared from homozygous jerker mice, which lack espin proteins owing to a mutation in their espin gene (Zheng et al., 2000; Sekerková et al., 2006a). Finally, among different rat and mouse tissues, there is a positive correlation between the signal the espin antibody gives on western blots or by immunocytochemistry and the levels of espin isoform mRNAs detected by RT-PCR (Sekerková et al., 2003, 2004).

The TuJ1 antibody (Covance, Emeryville, CA; Catalog number MMS-435P, Lot number 14892602) is a well-characterized mouse monoclonal antibody (IgG2a) that is highly selective for neuron-specific class III β-tubulin. It was raised against microtubules derived from rat brain and reacts with an epitope located in the extreme carboxy terminus of class III β-tubulin (Lee et al., 1990a, 1990b). The TuJ1 antibody specifically recognizes the ~50 kDa class III β-tubulin band on western blots of rat and chicken brain and labels neurons in sections prepared from a variety of mammalian and chicken tissues (Lee et al., 1990a, 1990b).

The synaptophysin antibody (Boehringer-Mannheim, Vienna, Austria; Catalog number 902 322, Lot number 1253028-03) is a mouse monoclonal antibody (IgG1) from clone SY38 mouse-mouse-hybrid cells. It was raised against a vesicular fraction prepared from bovine brain (Wiedenmann and Franke, 1985). The synaptophysin antibody reacts specifically with the 38-kDa synaptophysin band on western blots of rat and bovine brain and labels presynaptic terminals in sections prepared from a variety of mammalian tissues (Wiedenmann and Franke, 1985).

The peripherin antibodies were kindly provided by Dr. Gerry Shaw (University of Florida, Gainesville, FL), but are available commercially through EnCor Biotechnology, Inc. (Gainesville, FL). Peripherin is a class III intermediate filament protein found in sensory and other neurons, most of which are located in the peripheral nervous system (Barclay et al., 2007; Errante et al 1994, 1998; Hafidi, 1998). Mouse monoclonal peripherin antibody 7C5 (Catalog number MCA-7C5; IgG1), chicken polyclonal peripherin antibody (Catalog number RPCA-Peri) and rabbit polyclonal peripherin antibody (Catalog number CPCA-Peri) were raised against recombinant full-length rat peripherin isolated from *E. coli*. The

production and characterization of a similar antibody were described in Errante et al. (1994). All three peripherin antibodies react specifically with the 57-kDa peripherin band on western blots of rat brain and label peripherin-containing cells in sections prepared from a variety of mammalian tissues (manufacturer's technical information).

The lamin antibody is a rabbit polyclonal antibody (number 266) that was kindly provided by Dr. Robert and Anne Goldman (Northwestern University Feinberg School of Medicine, Chicago, IL). It was raised against recombinant full-length human lamin A isolated from *E. coli* (Moir et al., 1991). The antibody reacts specifically with the 70-kDa and 60-kDa bands of lamin A and C, respectively, on western blots and labels the nuclear lamina in a variety of mammalian cell lines (Moir et al., 1991, 1994).

Immunocytochemical analysis of cryosections

Adult rats and rats at postnatal day (P) 1 and P4 were deeply anesthetized by i.p. injections of sodium pentobarbital (60 mg/kg body weight) and transcardially perfused with 2% or 4% formaldehyde in 0.12 M phosphate buffer, pH 7.4. Embryos were harvested from timed-pregnant rats at embryonic day (E) 11.5, E12.5, E16 and E18 under deep sodium pentobarbital anesthesia (60 mg/kg body weight) and fixed in 2% formaldehyde in 0.12 M phosphate buffer, pH 7.4, for 1 hr. In rats at P5 and older, bony labyrinths were removed and decalcified in 10% EDTA/saline, while cochleas were dissected without decalcification from P1 and P4 rats. Cochleas and decalcified bony labyrinths were cryoprotected in 30% sucrose in phosphate-buffered saline, embedded in OCT compound (Electron Microscopy Sciences, Ft. Washington, PA) and cut on a cryostat microtome. Brainstem specimens were cryoprotected as specified and cut on a freezing-stage sliding microtome; serial coronal or sagittal sections, 25 μm-thick, were collected.

Sections were labeled using standard immunofluorescence or ABC immunoperoxidase methods as described elsewhere (Sekerková et al., 2005). Briefly, sections for immunoperoxidase labeling were incubated with 0.5 μg/ml of affinity purified polyclonal rabbit espin antibody or preimmune IgG. Bound antibody was detected using biotinylated donkey anti-rabbit IgG (Amersham Biosciences, Piscataway, NJ), the ABC Elite kit (Vector Laboratories, Burlingame, CA) and diaminobenzidine (Sigma). Some sections were further processed to enhance the DAB signal using the silver intensification protocol of Kitt et al. (1994). All stained sections were dehydrated, cleared and mounted in Entellan (Merck, Darmstadt, Germany).

Sections for immunofluorescence were incubated with the following primary antibodies, alone or in mixtures: affinity purified rabbit polyclonal espin antibody (1 μg/ml), TuJ1 mouse monoclonal class III β–tubulin antibody (1:800), mouse monoclonal synaptophysin antibody (1:1000), mouse monoclonal peripherin antibody (1:500), chicken polyclonal peripherin antibody (1:2000) or rabbit polyclonal peripherin antibody (1:1000). In experiments using TuJ1 antibody, which is highly sensitive to the degree of fixation (Sekerková et al., 2006a), we used mildly fixed samples (2% paraformaldehyde in phosphate buffered saline for ~ 30 min). Secondary antibodies were goat anti-rabbit IgG or goat anti-mouse IgG labeled with Alexa 488, 596, or 647 (Molecular Probes, Eugene, OR) or rhodamine-labeled donkey anti-chicken IgG (Jackson ImmunoResearch Laboratories, West Grove, PA). Sections were mounted with Vectashield (Vector Laboratories). Control sections processed with espin preimmune IgG or omission of primary antibody resulted in an absence of labeling.

Images were captured with a Spot RT CCD video camera (Diagnostics Instruments, Sterling Height, MI) mounted on a Nikon Eclipse 800 microscope using Spot RT Software 3.5.8. For confocal images, we used either a Nikon PCM2000 system with the Simple PCI Program or

a Zeiss LSM 510 META. All images were processed with Adobe Photoshop CS3 (upgraded from CS2) for adjustments of brightness and/or contrast.

Quantitative analysis

To estimate the percentage of espin–positive SGNs, the spiral ganglia of 3 rats were cut along their modiolar axis. Serial sections, 25 μm thick, were collected on gelatinized slides and double-labeled with espin and TuJ1 antibodies as described above. From each animal, every 10^{th} section was selected for quantification. We divided the cochlea into the hook region, the basal turn and the apical turn. From each spiral ganglion field, 1-μm-thick confocal images were taken using a 40× Plan-fluor lens with numerical aperture 1.3. The confocal setting was optimized to detect the SGNs with the lowest intensity of espin antibody labeling. Espin-positive and TuJ1-positive SGNs that included obvious nuclear profiles were counted on a computer screen using Adobe Photoshop CS2. The quantitative analysis included a total of 22 fields (4 hook regions, 10 basal turns, and 8 apical turns) from 9 cochlear sections, 3 sections from each animal. Raw cell counts were corrected for cell size using Abercrombie correction factors (Guillery, 2002) calculated from measurements of nuclear diameter (espin-positive, n= 59; espin-negative, n = 31) in 3 randomly chosen sections (1 for each animal) made using ImageJ (Abramoff et al., 2004; http://rsb.info.nih.gov/ij).

Western blots

For western blot analysis, 2 adult rats were euthanized by CO_2 inhalation and decapitation. Samples of CN, cerebellum and eye cup (i.e., eye with cornea, crystalline body and lens removed) were prepared by dissection. Tissues were homogenized in 20 volumes (ml/g of wet tissue) of 0.25 M sucrose, 3 mM imidazole-HCl, pH 7.4, containing 1 mM phenylmethylsulfonyl fluoride at 4°C using a 5-ml Potter-Elvehjem homogenizer (8 strokes, 3000 rpm) and immediately extracted at a concentration of ~20–40 mg wet tissue/ml by heating at 100°C in SDS gel sample buffer for 3 min, with intermittent agitation on a vortex mixer. Samples were centrifuged for 5 min at 16,000 × g in a microcentrifuge; the resulting supernates were resolved in SDS gels and analyzed on western blots using 0.2 μg/ml of affinity purified rabbit polyclonal espin antibody or preimmune IgG and the ECL system (Amersham Biosciences), with or without prior stripping according to the procedure recommended by the manufacturer. Duplicate control western blots were labeled with the rabbit preimmune IgG to distinguish bona fide espin isoform bands from non-specifically labeled bands, which can vary according to tissue source or developmental state (e.g., see Sekerková et al., 2006a). Films were scanned and imported into Adobe Photoshop CS3 with uniform adjustments of brightness and contrast.

RT-PCR

RNA was isolated from freshly dissected rat or mouse tissues using Trizol (Invitrogen) (Sekerková et al., 2003, 2004). For rats at P4, the entire membranous labyrinth was first isolated, and then the modiolar spiral ganglion region was carefully micro-dissected away from the remaining “sensory epithelium” fraction, which contains the hair cells. Adult human testis RNA was purchased from Clontech (Mountain View, CA). RT-PCR was carried out with selected espin primers in conjunction with kits and reagents purchased from Invitrogen. PCR products were subjected to DNA sequence analysis, either directly or after subcloning into the pEGFP-C1 vector (Clontech).

Cell transfection and labeling

The designated cell lines were plated on glass coverslips, transfected with expression plasmid constructs using Lipofectamine, fixed and examined by confocal microscopy as

described (Loomis et al., 2006; Sekerková et al., 2003). The different espin isoforms were prepared by RT-PCR and checked by DNA sequence analysis. GFP-espin constructs were inserted into the *Sma*I site of the pEGFP-C2 vector (Clontech), and untagged espin constructs were inserted into the *EcoR*V site of the pcDNA3 vector (Invitrogen). In some experiments, 10 nM leptomycin B (LC Laboratories, Woburn, MA) was added to block CRM1/Exportin1-mediated nuclear export (Kudo et al., 1999). To add the HIV Rev protein leucine-rich nuclear export signal, LQLPPLERLTL, between the GFP and the espin 3A+ coding sequences, the corresponding forward and reverse oligodeoxyribonucleotides (Integrated DNA Technologies, Coralville, IA) were converted to duplex form, phosphorylated on their 5′-ends with T4 polynucleotide kinase (New England Biolabs, Beverly, MA) and ligated in-frame into the *Bgl*II and *EcoR*I sites of the pEGFP-C2 multiple cloning site. The GFP-villin NT construct included the N-terminal 243-amino acid fragment of chicken villin (GenBank NM_205442) inserted into the *Kpn*I site of the pEGFP-C1 vector. 5′-phosphorylated, duplex oligodeoxyribonucleotides encoding the KVRILRHRK or RRSSSSTGKVRILRHRK espin peptides were ligated in-frame between the *BsrG*I and *Hind*III sites in the pEGFP-C1 multiple cloning site. In some experiments, fixed cells were briefly permeabilized with ice-cold 0.1% Triton X-100 and labeled with 4′-6-diamidino-2-phenylindole (DAPI) to localize chromatin and with espin antibody or rabbit polyclonal antibody to lamins A and C followed by Texas Red X-labeled goat anti-rabbit IgG $F(ab')_2$ fragment (Jackson ImmunoResearch Laboratories).

RESULTS

Espins in type-I SGNs and their central processes

When cryosections of decalcified adult rat inner ear were labeled with affinity purified rabbit polyclonal espin antibody, we found that espins were enriched in hair cell stereocilia (Fig. 1A–B″), in accordance with our previously published results (Zheng et al., 2000; Sekerková et al., 2004, 2006a). However, in addition, espin antibody labeling was detected in a large population of SGNs and their central processes, which were double-labeled with TuJ1 monoclonal antibody to neuron-specific, class III β-tubulin (Fig. 1A,A′,C-C″). In control sections stained with preimmune IgG, the SGNs were not labeled (Fig. 1D-D″). The labeling of the SGN cell bodies was even more intense than that observed in cerebellar Purkinje cells (Fig. 1A, inset a), which we showed previously to contain espins by multiple criteria (Sekerková et al., 2003). This labeling of SGNs was not noted in our previous study of rat inner ear (Sekerková et al., 2006a), because it focused on the analysis of cochlear whole-mounts, not cryosections, obtained from postnatal rats. The presence of espin transcripts and proteins in SGNs and their central processes was confirmed by RT-PCR and western blotting (see below under “SGN espin splice-isoforms with a functional NLS“). Remarkably, the espin antibody labeling was absent from the vestibular (Scarpa’s) ganglion neurons and their processes (Figs. 1A,A′,E-E″). Careful inspection of the confocal sections revealed that the espin antibody labeled both the cytoplasm and the nucleus of the SGNs (Fig. 1C-C″). Below we show that the nuclear labeling reflects the presence in SGNs of espin splice-isoforms that contain a functional NLS.

The type-II SGNs are selectively labeled by antibodies directed against the intermediate filament protein peripherin (Hafidi, 1998). When spiral ganglion sections were double-labeled with espin and peripherin antibodies, the peripherin-positive type-II SGNs were always espin-negative (Fig. 2A-A″, arrows), irrespective of position along Rosenthal’s canal. This indicated that the espins were present in only type-I SGNs. In sections double-labeled with TuJ1 and peripherin antibodies, we found that the type-I SGNs were intensely labeled with TuJ1 antibody, while the type-II SGNs, which could be recognized by their smaller size and labeling with peripherin antibody, reproducibly showed only faint labeling with TuJ1 antibody (Fig. 2B-B″, arrows). Dual labeling with the rabbit espin antibody and

the mouse TuJ1 monoclonal antibody was, therefore, an adequate means to identify the type-I SGNs and estimate the percentage of espin-positive type-I SGNs in sections. Quantitative analysis showed that 83 ±1% of the type-I SGNs contained espins, even though the intensity of espin antibody labeling varied from SGN to SGN within a section (Fig. 1C-C″). Examples of large SGNs intensely labeled with TuJ1 antibody but with no significant espin antibody labeling are shown with arrowheads in Fig. 1C-C″. Similar percentages of espin-positive type-I SGNs were detected in the hook region (80 ± 4 %), basal turn (81 ± 2%), and apical turn (86 ± 2%) of Rosenthal's canal, indicating that the presence of espin proteins is not correlated with tonotopic representation.

The espin antibody also labeled the central processes, or auditory nerve fibers (ANFs), of the SGNs (Fig. 1A,A′), however in these decalcified adult specimens labeling was not detected in the SGN peripheral processes, which innervate the inner hair cells (Fig. 1B-B″). This suggested that the espin proteins were preferentially distributed in the cell bodies and central processes of the espin-positive type-I SGNs in adults. In addition, the intensity of the espin antibody labeling in ANFs appeared to increase at the Schwann-glia border, where the cochlear nerve enters the CN (Fig, 1A,A′, dashed line in Fig. 1A′). ANFs observed entering the CN showed a pattern of espin antibody labeling identical to that in the cochlear sections: the thick ANFs of the type-I SGNs were labeled with espin antibody (Fig. 2C–D″), whereas the thinner, peripherin-positive ANFs of the type-II SGNs were espin-negative (Fig. 2C-C″, arrows). Here, too, the espin-positive ANFs represented a large proportion, but not all, of the ANFs labeled intensely with TuJ1 antibody (Fig. 2D-D″; arrows, examples of espin-negative, TuJ1-postive, large diameter ANFs). Taken together these data show a preferential distribution of espin proteins to the cell bodies and central processes of a large proportion of type-I SGNs.

Comparison of embryonic and postnatal specimens showed that the level of espin antibody labeling in SGNs increased dramatically during early postnatal development (Fig. 3B–D). As we showed previously, during early inner ear development, the espin antibody specifically labels the cytoplasmic compartment of otic epithelial cells, including the SGN precursors or neuroblasts, but this early espin protein expression is largely down-regulated upon neuroblast delamination (Sekerková et al., 2006a). Thus, robust espin antibody labeling was evident in the cytoplasm of otic epithelial cells at E12.5, but there was considerably less labeling in the developing vestibulocochlear ganglion (Fig. 3A-A′). An exception was the population of cells observed near the anteroventral wall of the otocyst, which exhibited a level of espin antibody labeling higher than in the rest of the ganglion (Fig. 3A″, arrows). On the basis of our previous studies (Sekerková et al., 2006a), these cells most likely represent recently delaminated neuroblasts that will experience a further down-regulation of their espins as they continue to undergo neuronal differentiation. At P1, the espin antibody labeling of SGNs appeared slightly more intense than at E18 (Fig. 3B–C′), but it was still faint in comparison to the intense signal in hair cells and in the cytoplasm of epithelial cells in the greater epithelial ridge (Fig. 3C,C′). At P4, the espin antibody labeling intensity in SGNs was dramatically increased (Fig. 3D,D′) and resembled that observed in decalcified adult specimens (Fig. 1C-C″). A large proportion of SGNs was labeled at P4 (Fig. 3D-D′), as in the adult. Beyond the labeling of SGN cell bodies, a weak labeling of SGN peripheral processes was detected in these non-decalcified specimens at P1 and P4 (Fig. 3C,C′,E,E′, arrowheads), in contrast to the absence of such labeling noted in decalcified adult specimens (Fig. 1B-B″). In mice, P3-P6 represents a time of SGN neurite retraction and synaptic pruning (Huang et al., 2007). Consistent with the assignment of espin-positive SGNs to type-I in adults (Fig. 2), the espin antibody labeled peripheral processes detected at P4 were mostly associated with the inner hair cells and seemed to be more prevalent on their modiolar face (Fig. 3E,E′).

Espins in ANFs and synaptic terminals in the CN

The espin antibody-labeled ANFs showed a distinctive pattern within the CN, with the most intense labeling in the central nerve root (CNR in Fig. 4B,E), followed closely by the central nerve root region (CNRR in Fig. 4B) and the octopus cell area in the PVCN (Fig. 4C,F). The other PVCN regions and the AVCN showed moderately intense labeling (Fig. 4A–C,E,F), while the DCN showed weaker labeling (Fig. 4B,C,F), which was confined to its deep layer (Fig. 4F,I). We did not detect any espin antibody labeling in the ventral, intermediate or dorsal acoustic stria. The espin-positive molecular layer of the cerebellum is also shown in Fig. 4A,B, where the espins are enriched in Purkinje cell dendritic spines (Sekerková et al., 2003). When the espin antibody was replaced by preimmune IgG, labeling was not detected in the CN or cerebellum (Fig. 4D).

In the ventral CN, the espin antibody labeled small en passant swellings and small and intermediate terminal boutons of the ANFs (Fig. 4G–J). This labeling of synaptic terminals was especially evident in the auditory nerve nucleus of the nerve root region and the octopus cell area of the PVCN. In these areas, the cell bodies of the root neurons (Fig. 4G, asterisk) and octopus cells (Fig. 4H, asterisks) were readily apparent because of their surrounding espin-positive boutons. The espin antibody labeled the surrounding boutons, and not the cell bodies, of the root neurons and octopus cells, as is clearly illustrated below using confocal immunofluorescence (see Fig. 5). In the DCN, numerous small en passant and terminal swellings were observed beneath the pyramidal cell layer in the deep layer (Fig. 4I). In contrast, the molecular layer of the DCN (Fig. 4I) and the different regions of the granule cell domain (Fig. 4F,J) were largely devoid of espin-positive fibers and boutons.

The idea of espin-positive afferent fibers extending into the central nervous system is not unique to the CN. We examined sections of the nose region and central nervous system with the purpose of identifying the central projections of the vomeronasal sensory neurons, which contain large amounts of espin proteins in their dendritic microvilli (Fig. 4K, arrowheads; see also Sekerková et al., 2004). Espin-positive bundles of vomeronasal nerve fibers were evident in the nasal connective tissue (Fig. 4K, arrows) and traveled caudally to the accessory olfactory bulb (Fig. 4L, arrow), where they terminated in glomeruli (Fig. 4L). These glomeruli were also labeled by espin antibody (Fig. 4L, arrowheads), suggesting that the terminal endings of the vomeronasal nerve fibers also contain espin proteins. Notably, in the central nervous system, espin antibody labeling was confined to SGN central projections in the CN, cerebellar Purkinje cells and the accessory olfactory bulb.

When the various regions of the CN were double-labeled with espin and TuJ1 antibodies and examined by confocal microscopy, we could clearly observe espin-positive synaptic endings around TuJ1-labeled neurons and dendrites. In the auditory nerve nucleus, the large spherical root neurons were surrounded by mid-sized espin-positive boutons (Fig. 5A, arrowheads). Numerous espin-positive boutons were also present in contact with the thick dendritic shaft of these neurons (Fig. 5A,B). This small group of neurons, which receives mostly, if not exclusively, primary acoustic inputs conveying high frequency sounds, consists of about 40–50 cells interspersed among the acoustic fibers (Lopez et al., 1993). Espin-positive boutons were also found in contact with globular bushy cells (Fig. 5C,D,I-I″) and multipolar neurons (Fig. 5F,H), however the number of espin-positive boutons contacting individual cells was less and varied from cell to cell. The cell bodies and dendrites of the specialized octopus cells, which are known to encode the timing of sound stimuli (Oertel, 1999), were densely innervated by espin-positive boutons (Fig. 5E). Unexpectedly, we observed only a few espin-positive boutons on spherical bushy cells in the AVCN (Fig. 5G). These cells receive primary inputs via the large endbulbs of Held, which are among the largest synaptic terminals in the central nervous system (Ryugo and Parks, 2003; Gentshev and Sotelo, 1973). In the AVCN of the cat, about 70% of the somatic

surface of spherical bushy cells is covered by synaptic terminals, roughly half of which arise from the cochlea (Cant and Morest, 1979). Nevertheless, in most instances, the tissue apposed to the cell bodies of spherical bushy cells in the rat AVCN did not label with espin antibody (Fig. 5G). To further demonstrate that the espin-positive boutons represented synaptic connections, we used double labeling with antibodies to espin and synaptophysin, a synaptic vesicle protein (De Camilli et al., 2000). As expected, the espin-positive terminals contacting the cell body and dendrites of CN neurons were double-labeled by synaptophysin antibody, as illustrated in Fig. 5H,I-I″.

SGN espin splice-isoforms with a functional NLS

Western blots and RT-PCR confirmed the presence of multiple espin isoforms and transcripts in SGNs. First, we looked for espin proteins on western blots of homogenate prepared from adult CN, which is relatively easy to isolate and is copiously innervated by espin-positive ANFs (Figs. 4,5). As a result of differential transcription start-site selection, the espin gene produces four major isoform size classes (numbered 1 through 4, in order of decreasing size), which can be readily distinguished on the basis of apparent molecular mass. Within an isoform size class, differential splicing produces additional variants, which show more subtle differences in apparent molecular mass (Sekerková et al., 2004). Western blots of CN homogenate contained multiple protein bands that labeled specifically with the affinity purified espin antibody (Fig. 6A). On the basis of apparent molecular mass and side-by-side comparisons with other tissues (eye and cerebellum) known to contain representative examples of the different espin isoform size classes, the major CN bands were assigned to the espin 3 isoforms (~32–35 kDa) and the espin 4 isoforms (~22–28 kDa) (Fig. 6A). Some espin 1 (~100–110 kDa) was also detected, and close inspection revealed two weaker bands in the positions expected for espin 2A (~60 kDa) and espin 2B (~65 kDa) (Fig. 6A). The latter were positioned on either side of a major nonspecific band, which was also labeled when preimmune IgG was substituted for the espin antibody (Fig. 6A). Note that the espin isoform bands were absent from the control western blots incubated with preimmune IgG (Fig. 6A).

Second, we used RT-PCR and DNA sequence analysis to examine espin transcripts in isolated rat spiral ganglion at P4. P4 was selected because it was much easier to micro-dissect the spiral ganglion region away from the sensory epithelium at P4 than in adult specimens and because high levels of espin proteins were already evident in SGNs at P4 by immunofluorescence (Fig. 3D,D′). We detected espin transcripts in total RNA prepared from isolated P4 spiral ganglion using a variety of espin-specific primers. For example, Fig. 6B shows the results obtained using comparable levels of total RNA prepared from isolated spiral ganglion and other selected tissues at P4 and espin primers from exons w and z (Fig. 6C), which detect all known espin isoforms. DNA sequence analysis of the RT-PCR products obtained from isolated P4 spiral ganglion revealed a mixture of espin transcripts with and without the 27-nt exon s (Fig. 6C) (Sekerková et al., 2003). When the RT-PCR products obtained using primers from exons r and w (Fig. 6C) were ligated into a vector, used to transform bacteria and the resulting clones sequenced individually, one-third (4 out of 12) were found to contain the 27-nt exon s insert. Exon s encodes a short, 9-amino acid peptide, which is rich in positively charged amino acids: KVRILRHRK (Fig. 6C). RT-PCR analysis of total RNA from mouse inner ear and cerebellum (Sekerková et al., 2003, 2004) and adult human testis uncovered espin transcripts that included a homologous exon and encoded a highly similar nonapeptide; the only difference was a conservative substitution of a V for the I in the rat sequence (Fig. 6C).

Because it was rich in positively charged amino acids, the KVRILRHRK nonapeptide resembled an NLS, which signals importin/karyopherin-mediated nuclear import (Lange et al., 2007). Therefore, we wondered whether it might account for our detection of espin

antibody labeling in the nucleus of SGNs. This nuclear labeling was especially evident by confocal immunofluorescence analysis of sections double-labeled with espin and TuJ1 antibodies, in which the TuJ1 labeling was confined to the cytoplasmic compartment (Fig. 6D,D′; see also Fig. 1C-C″). To examine its nuclear targeting potential, we compared the localization of espin constructs with and without this nonapeptide in a variety of transfected cell lines. The presentation of our results in Fig. 6D-N highlights our experiments with subconfluent renal LLC-PK1 epithelial cells because of their ease of handling, but identical results were obtained using neuronal (Neuro2a, PC12) and fibroblastic (BHK) cell lines (data not shown). Without the nonapeptide, GFP-espin 3A (Fig. 6C) became localized to coarse actin bundles in the cytoplasm (Fig. 6E,E′), as we have observed previously for a variety of espin isoforms when expressed in well-spread tissue culture cells that display a fibroblast-like morphology (Bartles et al., 1998; Chen et al., 1999; Loomis et al., 2006). In contrast, the corresponding construct that included the KVRILRHRK nonapeptide, GFP-espin 3A+ (Fig. 6C), became efficiently localized to the nucleus (Fig. 6F,F′), although a small fraction also localized to cytoplasmic actin bundles (upper left in Fig. 6F). As observed in high-magnification confocal images of transfected cells labeled with lamin antibody, the GFP-espin 3A+ was found to be internal to the nuclear lamina and, hence, was inside the nucleus and not merely adsorbed to the nuclear surface (Fig. 6G). In transfected cells double-labeled with DAPI to localize chromatin, the intranuclear GFP-espin 3A+ showed enrichment in the interchromatin space, which was deficient in DAPI labeling (Fig. 6H-H″). Reduced GFP-espin 3A+ accumulation was also noted in nucleoli (Fig. 6F–H). Efficient nuclear accumulation was also observed for GFP-human espin 3A+ (data not shown), in which the nonapeptide sequence contains the conservative I-to-V substitution (Fig. 6C), and for a variety of untagged rat espin isoforms that included the nonapeptide, including espin 3B+, espin 2A+ and espin 2B+, the latter being detected with espin antibody. The results for the untagged espin 2B constructs are shown in Fig. 6I–J′. Without the nonapeptide, untagged espin 2B (Fig. 6C) became localized to coarse actin bundles in the cytoplasm (Fig. 6I,I′), but the corresponding construct containing the nonapeptide, espin 2B+ (Fig. 6C), was efficiently localized to the nucleus (Fig. 6J,J′). Curiously, GFP-tagged versions of espin 2B+ and espin 2A+ did not localize to the nucleus, suggesting that for these isoforms the presence of the GFP tag somehow interfered with nuclear accumulation.

These experiments suggested that the nonapeptide was functioning as an NLS that caused the selective nuclear accumulation of espin isoforms that contained it. Accumulation in the nucleus typically reflects a balance between nuclear import and export (Kutay and Guttinger, 2005; Lange et al., 2007). Upon visual inspection, the espin isoforms did not contain any recognizable leucine-rich consensus sequences for CRM1/Exportin 1-mediated nuclear export: Φ-X_{2-3}-Φ-X_{2-3}-Φ-X-Φ (Φ= L,I,V,F,M, where X = any amino acid; Kutay and Guttinger, 2005). Accordingly, inclusion of the CRM1/Exportin inhibitor leptomycin B (10 ng/ml) for 1–8 h prior to fixation (Kudo et al., 1999) had no affect on the localization of GFP-espin 3A or GFP-espin 3A+ in the transfected cells (data not shown). This suggested that the cytoplasmic localization of GFP-espin 3A (i.e., the isoform lacking the nonapeptide) is not the result of highly efficient CRM1/Exportin-mediated nuclear export. It also suggested that espin 3A does not contain an NLS. We were, however, able to drastically reduce the nuclear accumulation of GFP-espin 3A+ by adding a single copy of the leucine-rich HIV Rev protein nuclear export signal, LQLPPLERLTL (Kutay and Guttinger, 2005), between the GFP and the espin 3A+ (Fig. 6K,K′).

To ascertain whether the KVRILRHRK nonapeptide was sufficient to cause the nuclear localization of an unrelated protein, we developed a cell transfection assay examining the subcellular localization of GFP-Villin NT, a GFP fusion with the N-terminal 243-amino acid fragment of chicken villin, which includes the two N-terminal gelsolin-like repeats. GFP without the villin fragment is not suitable for these types of nuclear targeting experiments,

because it tends to concentrate in the nucleus to a significant extent without any added NLS. In transfected cells, the GFP-Villin NT was predominantly cytoplasmic (Fig. 6L). Insertion of the KVRILRHRK nonapeptide between the GFP and villin N-terminal fragment had no effect: this construct was also predominantly cytoplasmic (Fig. 6M). However, insertion of the KVRILRHRK nonapeptide together with the RRSSSSTG octapeptide positioned immediately upstream of the nonapeptide in the espin sequence (Fig. 6C, blue) resulted in efficient nuclear accumulation (Fig. 6N). Thus, this 17-amino acid peptide was sufficient to cause nuclear localization of the GFP-villin fragment. Because the upstream octapeptide included two positively charged residues (the two arginines marked with blue asterisks in Fig. 6C), these results suggested that the KVRILRHRK nonapeptide contributes to a bipartite NLS (Lange et al., 2007), consisting of the two arginine residues in the upstream peptide encoded by exon r and the positively charged nonapeptide encoded by exon s (Fig. 6C).

DISCUSSION

Our discovery of espin transcripts and proteins in rat type-I SGNs suggests additional roles for these multifunctional actin-cytoskeletal proteins in auditory neuroscience beyond their better-characterized roles in hair cell stereocilium elongation, length regulation and integrity (Zheng et al., 2000; Loomis et al., 2003; Rzadzinska et al., 2005; Sekerková et al., 2006a, 2006b). A common theme among espin-rich sensory and neuronal cells is Ca^{2+}-based signaling (Sekerková et al., 2003, 2004, 2006a). Espins differ from many other actin-bundling proteins, such as fimbrins/plastins and villin, in that they are not inhibited by Ca^{2+} (Bartles et al., 1998; Chen et al., 1999; Sekerková et al., 2004). SGNs contain calcium channels and nonspecific cation channels and show increased Ca^{2+} uptake in response to a variety of stimuli (e.g., Hisashi et al., 1995; Shimozono et al., 1995; Housley et al., 1999; Lopez et al., 2003; Yukawa et al., 2005; Greenwood et al., 2007; Xie et al., 2007). Thus, although SGNs are not known to contain large, stable PABs like those found in hair cell stereocilia, we propose that SGN espins may be acting in part to supply Ca^{2+}-resistant cross-links to stabilize smaller-scale, looser and possibly more dynamic actin assemblies. These may, in turn, be involved in key actin-dependent processes in these neurons, such as morphogenesis and structural plasticity (Luo, 2002), axonal transport (Hollenbeck and Saxton, 2005) or scaffolding of synaptic regulatory molecules (Sankaranarayanan et al., 2003).

Our detection of espin proteins in type-I SGNs, but not type-II SGNs or vestibular ganglion neurons, suggests roles for espins in afferent signaling between a specific class of inner ear sensory cell, the inner hair cells, and their target neurons in the CN. Type-I SGNs are arranged tonotopically along the cochlea and display a characteristic frequency, which varies from high to low as one proceeds from base to apex along the spiral (reviewed in Ryugo and Parks, 2003). SGNs in different locations differ electrophysiologically. For example, mouse basal SGNs show short latency, rapidly adapting responses, whereas apical SGNs show longer latency, slowly adapting responses (Adamson et al., 2002). SGN action potential thresholds are distributed nonmonotonically, so that those in the middle region show the greatest sensitivity (Liu and Davis, 2007). Our detection of a similar percentage of espin-positive type-I SGNs in the hook region, base and apex of the cochlea suggests no obvious correlation between espin presence and characteristic frequency or these other electrophysiological parameters, although a correlation with espin levels or espin isoform distributions cannot presently be excluded. Type-I ANFs are also categorized according to spontaneous discharge rate (Ryugo and Parks, 2003; Taberner and Liberman, 2005), but our detection of espin proteins in over 80% of the type-I SGNs also does not correlate well with this parameter. Therefore, espin protein expression may distinguish a previously unrecognized category of rat type-I SGNs.

The expression of espin proteins in type-I SGNs poses intriguing problems in gene expression. During early inner ear development, espin proteins are expressed at relatively high levels throughout the otic epithelium, including the SGN precursors (the neuroblasts), but are down regulated upon neuroblast delamination (Sekerková et al., 2006a). Then SGN espin protein levels rise again in a large subpopulation of type-I SGNs during early postnatal life. Little is known about stimuli that can regulate espin levels, except in the male reproductive system, where high levels of espin expression depend on testosterone and possibly also gonadotrophic hormones (Show et al., 2004; Primiani et al., 2007). Regulation of espin gene expression may be complicated by the existence of multiple transcription starts sites (Sekerková et al., 2004) and, hence, the possibility that different promoters are involved. In addition, differential splicing is required to produce the NLS-containing espin isoforms, which most likely account for the espin antibody labeling we detect in nucleus of SGNs. The level of espin proteins in developing SGNs increases dramatically between P0 and P4. This corresponds to the time when SGN-hair cell connections are being refined, through the pruning of synapses and retraction of neurites (Huang et al., 2007), processes which may involve ATP-gated, Ca^{2+}-mediated signaling through specific SGN P2X receptors (Greenwood et al., 2007). Thus, SGN espin levels are already elevated during the period of spontaneous ATP-mediated signaling, which takes place before the onset of hearing (Tritsch et al., 2007).

Our detection of espins in a majority of type-I SGNs brings the number of espin-expressing neurons identified to three – Purkinje cells, vomeronasal sensory neurons and SGNs – and solidifies the idea that espins are not confined to epithelial cells. Remarkably, the localization of espin proteins appears to differ significantly among neuron types. In Purkinje cells, espins are concentrated postsynaptically, in dendritic spines (Sekerková et al., 2003). In vomeronasal sensory neurons, espins are concentrated in the PABs of the dendritic microvilli (Sekerková et al., 2004) and, as shown in the present study, in their axons projecting to the glomeruli of the accessory olfactory bulb. In SGNs, espin proteins appear concentrated in the cell body, including the cell nucleus, and also in their central processes projecting to different types of large CN neurons that give rise to multiple channels directed to the upper auditory brainstem. Although the espin-positive ANFs show a projection pattern typical of type-I SGNs (Ryugo and Parks, 2003), the espin proteins are detected at high levels in only a subset of synaptic terminals, e.g., those around nerve root neurons and octopus cells in the PVCN. Remarkably, the espin antibody did not appear to label the typical large endbulbs of Held on the spherical bushy cells in the AVCN. As each ANF may give rise to 1–2 endbulbs of Held (Ryugo and Parks, 2003), the data suggest an additional form of espin compartmentalization within the central processes to a subset of presynaptic terminals.

Our detection of espin antibody labeling in the nucleus of SGNs led to the discovery of another form of espin compartmentalization, which involves espin splice-isoforms that contain a functional NLS. Thus far, we have noticed large amounts of nuclear espin antibody labeling only in SGNs, although we previously observed low levels of specific espin antibody labeling in the nucleus of taste bud sensory cells (Sekerková et al., 2005). One-third of the espin transcripts in isolated P4 spiral ganglion include the 27-nt exon s, which encodes the KVRILRHRK nonapeptide that contributes to the bipartite NLS. We noticed exon s previously in a subset of espin transcripts in the cerebellum, but did not recognize its significance (Sekerková et al., 2003). In the present study, we demonstrated that the nonapeptide engenders a bipartite NLS that is functional in a variety of transfected cell lines, including two neuronal cell lines. The intense, specific labeling we observed in the SGN nucleus with the espin antibody argues strongly that this NLS is also functional in rat type-I SGNs. The detection of this functional NLS in espin splice-isoforms adds a new dimension to espin biology. Actin or actin-related proteins are known to be involved in

multiple aspects of nuclear biology, including RNA transcription, processing and export; chromatin remodeling; nucleoskeletal organization; and nucleocytoplasmic transport (Bettinger et al., 2004; Pederson and Aebi, 2005; Miralles and Visa, 2006). The NLS-bearing espin splice-isoforms join a growing list of actin-cytoskeletal proteins that can accumulate in the nucleus, e.g., the actin monomer-regulated transcriptional co-activator MAL (Vartiainen et al., 2007), the actin nucleation-promoting factor N-WASP (Wu et al., 2006), the actin monomer-binding protein profilin (Stüven et al., 2003; Birbach et al., 2006), the unconventional myosin motors nuclear myosin I and myosin VI (Pestic-Dragovich et al., 2000; Vreugde et al., 2006) and the actin-bundling proteins myopodin and the plastins (Weins et al., 2001; Delanote et al., 2005). Most nuclear actin is believed to exist in monomeric, oligomeric or unconventional forms (Pederson and Aebi, 2002, 2005; Jockusch et al., 2006; McDonald et al., 2006). Espins are multifunctional proteins, which in addition to cross-linking actin filaments and elongating PABs, can bind other ligands implicated in actin-cytoskeletal regulation or signaling (Sekerková et al., 2004, 2006a, 2006b). For example, we have shown that espins bind monomeric actin via their WH2 domain (Loomis et al., 2006) and, thus, might affect the delivery, sequestration or localization of monomeric nuclear actin or actin-related proteins. Espin isoforms large enough to include exon s also contain 1 or 2 proline-rich peptides, which we have shown to bind the profilins (Loomis et al., 2003; Sekerková et al., 2004). Profilins, which have been implicated in synaptic vesicle exocytosis, neuronal excitability and mouse novelty-seeking behavior (Pilo Boyl et al., 2007), can regulate nuclear actin levels, via a dedicated exportin (Stüven et al., 2003), as well as transcription factor activity (Lederer et al., 2005). Thus, these newly discovered NLS-containing espin splice-isoforms have the potential to regulate actin-based nuclear processes at multiple levels and may even relay information between the SGN cytoplasm and nucleus.

Supplementary Material

Refer to Web version on PubMed Central for supplementary material.

Acknowledgments

We thank Dr. Gerry Shaw for peripherin antibodies, Dr. Robert and Anne Goldman for lamin antibody, Dr. Patricia A. Loomis for initial studies on nuclear targeting, and Dr. Donna S. Whitlon and Dr. Stephen Adam for valuable discussions.

Grant sponsor: National Institute on Deafness and Other Communication Disorders; Grant number: R01 DC004314 (to J.R.B.)

LITERATURE CITED

Abramoff MD, Magelhaes PJ, Ram SJ. Image processing with Image. J Biophotonics International. 2004; 11:36–42.

Adamson CL, Reid MA, Mo ZL, Bowne-English J, Davis RL. Firing features and potassium channel content of murine spiral ganglion neurons vary with cochlear location. J Comp Neurol. 2002; 447:331–350. [PubMed: 11992520]

Barclay M, Noakes PG, Ryan AF, Julien JP, Housley GD. Neuronal expression of peripherin, a type III intermediate filament protein, in the mouse hindbrain. Histochem Cell Biol. 2007; 128:541–550. [PubMed: 17899157]

Bartles JR, Zheng L, Li A, Wierda A, Chen B. Small espin: a third actin-bundling protein and potential forked protein ortholog in brush border microvilli. J Cell Biol. 1998; 143:107–119. [PubMed: 9763424]

Bettinger BT, Gilbert DM, Amberg DC. Actin up in the nucleus. Nat Rev Mol Cell Biol. 2004; 5:410–415. [PubMed: 15122354]

Birbach A, Verkuyl JM, Matus A. Reversible, activity-dependent targeting of profilin to neuronal nuclei. Exp Cell Res. 2006; 312:2279–2287. [PubMed: 16716297]

Bourk TR, Mielcarz JP, Norris BE. Tonotopic organization of the anteroventral cochlear nucleus of the cat. Hear Res. 1981; 4:215–241. [PubMed: 7263511]

Cant NB, Morest DK. The bushy cells in the anteroventral cochlear nucleus of the cat. A study with the electron microscope. Neuroscience. 1979; 4:1925–1945. [PubMed: 530439]

Chen B, Li A, Wang D, Wang M, Zheng L, Bartles JR. Espin contains an additional actin-binding site in its N terminus and is a major actin-bundling protein of the Sertoli cell-spermatid ectoplasmic specialization junctional plaque. Mol Biol Cell. 1999; 10:4327–4339. [PubMed: 10588661]

De Camilli, P.; Haucke, V.; Takei, K.; Mugnaini, E. The structure of synapses. In: Cowan, M.; Südhof, T.; Stevens, C., editors. Synapses. Baltimore: John Hopkins University Press; 2000. p. 89-133.

Delanote V, Van Impe K, De Corte V, Bruyneel E, Vetter G, Boucherie C, Mareel M, Vandekerckhove J, Friederich E, Gettemans J. Molecular basis for dissimilar nuclear trafficking of the actin-bundling protein isoforms T- and L-plastin. Traffic. 2005; 6:335–345. [PubMed: 15752138]

Donaudy F, Zheng L, Ficarella R, Ballana E, Carella M, Melchionda S, Estivill X, Bartles JR, Gasparini P. Espin gene (ESPN). mutations associated with autosomal dominant hearing loss cause defects in microvillar elongation or organisation. J Med Genet. 2006; 43:157–161. [PubMed: 15930085]

Errante L, Tang D, Gardon M, Sekerková G, Mugnaini E, Shaw G. The intermediate filament protein peripherin is a marker for cerebellar climbing fibres. J Neurocytol. 1998; 27:69–84. Erratum in: J Neurocytol 1998 27: 281–288. [PubMed: 9609398]

Errante LD, Wiche G, Shaw G. Distribution of plectin, an intermediate filament-associated protein, in the adult rat central nervous system. J Neurosci Res. 1994; 37:515–528. [PubMed: 8021973]

Gentschev T, Sotelo C. Degenerative patterns in the ventral cochlear nucleus of the rat after primary deafferentation. An ultra-structural study. Brain Res. 1973; 62:37–60. [PubMed: 4765119]

Greenwood D, Jagger DJ, Huang LC, Hoya N, Thorne PR, Wildman SS, King BF, Pak K, Ryan AF, Housley GD. P2X receptor signaling inhibits BDNF-mediated spiral ganglion neuron development in the neonatal rat cochlea. Development. 2007; 134:1407–1417. [PubMed: 17329369]

Guillery RW. On counting and counting errors. J Comp Neurol. 2002; 447:1–7. [PubMed: 11967890]

Hafidi A. Peripherin-like immunoreactivity in type II spiral ganglion cell body and projections. Brain Res. 1998; 805:181–190. [PubMed: 9733963]

Hisashi K, Nakagawa T, Yasuda T, Kimitsuki T, Komune S, Komiyama S. Voltage-dependent Ca^{2+} channels in the spiral ganglion cells of guinea pig cochlea. Hear Res. 1995; 91:196–201. [PubMed: 8647721]

Hollenbeck PJ, Saxton WM. The axonal transport of mitochondria. J Cell Sci. 2005; 118:5411–5419. [PubMed: 16306220]

Housley GD, Kanjhan R, Raybould NP, Greenwood D, Salih SG, Jarlebark L, Burton LD, Setz VC, Cannell MB, Soeller C, Christie DL, Usami S, Matsubara A, Yoshie H, Ryan AF, Thorne PR. Expression of the $P2X_2$ receptor subunit of the ATP-gated ion channel in the cochlea: implications for sound transduction and auditory neurotransmission. J Neurosci. 1999; 19:8377–8388. [PubMed: 10493739]

Huang LC, Thorne PR, Housley GD, Montgomery JM. Spatiotemporal definition of neurite outgrowth, refinement and retraction in the developing mouse cochlea. Development. 2007; 134:2925–2933. [PubMed: 17626062]

Jockusch BM, Schoenenberger CA, Stetefeld J, Aebi U. Tracking down the different forms of nuclear actin. Trends Cell Biol. 2006; 16:391–396. [PubMed: 16828286]

Kiang NY, Rho JM, Northrop CC, Liberman MC, Ryugo DK. Hair-cell innervation by spiral ganglion cells in adult cats. Science. 1982; 217:175–177. [PubMed: 7089553]

Kitt CA, Hohmann C, Coyle JT, Price DL. Cholinergic innervation of mouse forebrain structures. J Comp Neurol. 1994; 341:117–129. [PubMed: 8006218]

Kudo N, Matsumori N, Taoka H, Fujiwara D, Schreiner EP, Wolff B, Yoshida M, Horinouchi S. Leptomycin B inactivates CRM1/exportin 1 by covalent modification at a cysteine residue in the central conserved region. Proc Natl Acad Sci U S A. 1999; 96:9112–9117. [PubMed: 10430904]

Kutay U, Guttinger S. Leucine-rich nuclear-export signals: born to be weak. Trends Cell Biol. 2005; 15:121–124. [PubMed: 15752974]

Lange A, Mills RE, Lange CJ, Stewart M, Devine SE, Corbett AH. Classical nuclear localization signals: definition, function, and interaction with importin alpha. J Biol Chem. 2007; 282:5101–5105. [PubMed: 17170104]

Lederer M, Jockusch BM, Rothkegel M. Profilin regulates the activity of p42POP, a novel Myb-related transcription factor. J Cell Sci. 2005; 118:331–341. [PubMed: 15615774]

Lee MK, Rebhun LI, Frankfurter A. Posttranslational modification of class III beta-tubulin. Proc Natl Acad Sci U S A. 1990a; 87:7195–7199. [PubMed: 2402501]

Lee MK, Tuttle JB, Rebhun LI, Cleveland DW, Frankfurter A. The expression and posttranslational modification of a neuron-specific beta-tubulin isotype during chick embryogenesis. Cell Motil Cytoskeleton. 1990a; 17:118–132. [PubMed: 2257630]

Liu Q, Davis RL. Regional Specification of Threshold Sensitivity and Response Time in CBA/CaJ Mouse Spiral Ganglion Neurons. J Neurophysiol. 2007; 98:2215–2222. [PubMed: 17715200]

Loomis PA, Zheng L, Sekerková G, Changyaleket B, Mugnaini E, Bartles JR. Espin cross-links cause the elongation of microvillus-type parallel actin bundles in vivo. J Cell Biol. 2003; 163:1045–1055. [PubMed: 14657236]

Loomis PA, Kelly AE, Zheng L, Changyaleket B, Sekerková G, Mugnaini E, Ferreira A, Mullins RD, Bartles JR. Targeted wild-type and jerker espins reveal a novel, WH2-domain-dependent way to make actin bundles in cells. J Cell Sci. 2006; 119:1655–1665. [PubMed: 16569662]

Lopez, DE.; Merchan, MA.; Bajo, VM.; Saldana, E. The cochlear root neurons in the rat, mouse and gerbil. The mammalian cochlear nuclei. In: Merchan, MA.; Juiz, JM.; Godfrey, DA.; Mugnaini, E., editors. Organization and function. New York: Plenum Press; 1993. p. 291-301.

Lopez I, Ishiyama G, Acuna D, Ishiyama A, Baloh RW. Immunolocalization of voltage-gated calcium channel alpha1 subunits in the chinchilla cochlea. Cell Tissue Res. 2003; 313:177–186. [PubMed: 12845523]

Luo L. Actin cytoskeleton regulation in neuronal morphogenesis and structural plasticity. Annu Rev Cell Dev Biol. 2002; 18:601–635. [PubMed: 12142283]

McDonald D, Carrero G, Andrin C, de Vries G, Hendzel MJ. Nucleoplasmic beta-actin exists in a dynamic equilibrium between low-mobility polymeric species and rapidly diffusing populations. J Cell Biol. 2006; 172:541–552. [PubMed: 16476775]

Miralles F, Visa N. Actin in transcription and transcription regulation. Curr Opin Cell Biol. 2006; 18:261–266. [PubMed: 16687246]

Moir RD, Donaldson AD, Stewart M. Expression in Escherichia coli of human lamins A and C: infludence of head and tail domains on assembly properties and paracrystal formation. J Cell Sci. 1991; 99:363–372. [PubMed: 1885674]

Moir RD, Montag-Lowy M, Goldman RD. Dynamic properties of nuclear lamins: lamin B is associated with sites of DNA replication. J Cell Biol. 1994; 125:1201–1212. [PubMed: 7911470]

Naz S, Griffith AJ, Riazuddin S, Hampton LL, Battey JF Jr, Khan SN, Riazuddin S, Wilcox ER, Friedman TB. Mutations of ESPN cause autosomal recessive deafness and vestibular dysfunction. J Med Genet. 2004; 41:591–595. [PubMed: 15286153]

Oertel D. The role of timing in the brain stem auditory nuclei of vertebrates. Annu Rev Physiol. 1999; 61:497–519. [PubMed: 10099699]

Pederson T, Aebi U. Actin in the nucleus: what form and what for? J Struct Biol. 2002; 140:3–9. [PubMed: 12490148]

Pederson T, Aebi U. Nuclear actin extends, with no contraction in sight. Mol Biol Cell. 2005; 16:5055–5060. [PubMed: 16148048]

Pestic-Dragovich L, Stojiljkovic L, Philimonenko AA, Nowak G, Ke Y, Settlage RE, Shabanowitz J, Hunt DF, Hozak P, de Lanerolle P. A myosin I isoform in the nucleus. Science. 2000; 290:337–341. [PubMed: 11030652]

Pilo Boyl P, Di Nardo A, Mulle C, Sassoe-Pognètto M, Panzanelli P, Mele A, Kneussel M, Constantini V, Perlas E, Massimi M, Vara H, Giustetto M, Witke W. Profilin2 contributes to synaptic vesicle exocytosis, neuronal excitability, and novelty-seeking behavior. EMBO J. 2007; 26:2991–3002. [PubMed: 17541406]

Primiani N, Gregory M, Dufresne J, Smith CE, Liu YL, Bartles JR, Cyr DG, Hermo L. Microvillar size and espin expression in principal cells of the adult rat epididymis are regulated by androgens. J Androl. 2007; 28:659–669. [PubMed: 17409466]

Rubel EW, Fritzsch B. Auditory system development: primary auditory neurons and their targets. Annu Rev Neurosci. 2002; 25:51–101. [PubMed: 12052904]

Ryugo, DK. The auditory nerve: Peripheral innervaton, cell body morphology, and central projections. In: Webster, DB.; Popper, AN.; Fay, RR., editors. The mammalian auditory pathway: neuroanatomy. New York: Springer-Verlag; 1992. p. 23-65.

Ryugo DK, Parks TN. Primary innervation of the avian and mammalian cochlear nucleus. Brain Res Bull. 2003; 60:435–456. [PubMed: 12787866]

Rzadzinska A, Schneider M, Noben-Trauth K, Bartles JR, Kachar B. Balanced levels of Espin are critical for stereociliary growth and length maintenance. Cell Motil Cytoskeleton. 2005; 62:157–165. [PubMed: 16206170]

Sankaranarayanan S, Atluri PP, Ryan TA. Actin has a molecular scaffolding, not propulsive, role in presynaptic function. Nat Neurosci. 2003; 6:127–135. [PubMed: 12536209]

Sekerková G, Freeman D, Mugnaini E, Bartles JR. Espin cytoskeletal proteins in the sensory cells of rodent taste buds. J Neurocytol. 2005; 34:171–182. [PubMed: 16841162]

Sekerková G, Zheng L, Mugnaini E, Bartles JR. Differential expression of espin isoforms during epithelial morphogenesis, stereociliogenesis and postnatal maturation in the developing inner ear. Dev Biol. 2006a; 291:83–95.

Sekerková G, Zheng L, Loomis PA, Mugnaini E, Bartles JR. Espins and the actin cytoskeleton of hair cell stereocilia and sensory cell microvilli. Cell Mol Life Sci. 2006b; 63:2329–2341.

Sekerková G, Zheng L, Loomis PA, Changyaleket B, Whitlon DS, Mugnaini E, Bartles JR. Espins are multifunctional actin cytoskeletal regulatory proteins in the microvilli of chemosensory and mechanosensory cells. J Neurosci. 2004; 24:5445–5456. [PubMed: 15190118]

Sekerková G, Loomis PA, Changyaleket B, Zheng L, Eytan R, Chen B, Mugnaini E, Bartles JR. Novel espin actin-bundling proteins are localized to Purkinje cell dendritic spines and bind the Src homology 3 adapter protein insulin receptor substrate p53. J Neurosci. 2003; 23:1310–1319. [PubMed: 12598619]

Shimozono M, Tono T, Morimitsu T, Nakagawa T, Komune S. Measurement of intracellular free Ca^{2+} concentration in guinea pig spiral ganglion cells. Neuroreport. 1995; 6:421–424. [PubMed: 7766835]

Show MD, Anway MD, Zirkin BR. An ex vivo analysis of Sertoli cell actin dynamics following gonadotropic hormone withdrawal. J Androl. 2004; 25:1013–1021. [PubMed: 15477377]

Stüven T, Hartmann E, Görlich D. Exportin 6: a novel nuclear export receptor that is specific for profilin-actin complexes. EMBO J. 2003; 22:5928–5940. [PubMed: 14592989]

Taberner AM, Liberman MC. Response properties of single auditory nerve fibers in the mouse. J Neurophysiol. 2005; 93:557–569. [PubMed: 15456804]

Tritsch NX, Yi E, Gale JE, Glowatzki E, Bergles DE. The origin of spontaneous activity in the developing auditory system. Nature. 2007; 450:50–55. [PubMed: 17972875]

Vartiainen MK, Guettler S, Larijani B, Treisman R. Nuclear actin regulates dynamic subcellular localization and activity of the SRF cofactor MAL. Science. 2007; 316:1749–1752. [PubMed: 17588931]

Vreugde S, Ferrai C, Miluzio A, Hauben E, Marchisio PC, Crippa MP, Bussi M, Biffo S. Nuclear myosin VI enhances RNA polymerase II-dependent transcription. Mol Cell. 2006; 23:749–755. [PubMed: 16949370]

Weins A, Schwarz K, Faul C, Barisoni L, Linke WA, Mundel P. Differentiation- and stress-dependent nuclear cytoplasmic redistribution of myopodin, a novel actin-bundling protein. J Cell Biol. 2001; 155:393–404. [PubMed: 11673475]

Wiedenmann B, Franke WW. Identification and localization of synaptophysin, an integral membrane glycoprotein of Mr 38,000 characteristic of presynaptic vesicles. Cell. 1985; 41:1017–1028. [PubMed: 3924408]

Wu X, Yoo Y, Okuhama NN, Tucker PW, Liu G, Guan JL. Regulation of RNA-polymerase-II-dependent transcription by N-WASP and its nuclear-binding partners. Nat Cell Biol. 2006; 8:756–763. [PubMed: 16767080]

Xie D, Hu P, Xiao Z, Wu W, Chen Y, Xia K. Subunits of voltage-gated calcium channels in murine spiral ganglion cells. Acta Otolaryngol. 2007; 127:8–12. [PubMed: 17364322]

Yukawa H, Shen J, Harada N, Cho-Tamaoka H, Yamashita T. Acute effects of glucocorticoids on ATP-induced Ca^{2+} mobilization and nitric oxide production in cochlear spiral ganglion neurons. Neuroscience. 2005; 130:485–496. [PubMed: 15664705]

Zheng L, Sekerková G, Vranich K, Tilney LG, Mugnaini E, Bartles JR. The deaf jerker mouse has a mutation in the gene encoding the espin actin-bundling proteins of hair cell stereocilia and lacks espins. Cell. 2000; 102:377–385. [PubMed: 10975527]

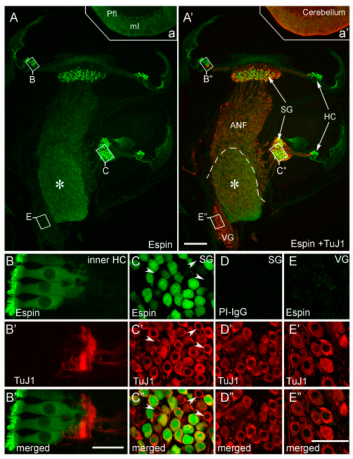

Fig 1.

Immunofluorescence localization of espins in cryosections of adult rat cochlea. Sections of decalcified inner ear labeled with affinity purified rabbit polyclonal espin antibody or preimmune IgG (PI-IgG) (green) and TuJ1 class III β-tubulin antibody (red). **A,A′**: Intense espin antibody labeling is present in hair cells (HC), in neurons of the spiral ganglion (SG) and in their auditory nerve fibers (ANF). Neurons of the vestibular ganglion (VG) are not labeled with espin antibody. The Schwann-glia border is shown with a dashed line in A′, and the asterisk in A,A′ marks the central nervous system portion of the ANFs, which shows elevated espin antibody labeling. A portion of the cerebellar paraflocculus lobule (Pfl) that was processed together with the cochlear tissue in the temporal bone is shown in insets a,a′. Espin antibody labels the cerebellar Purkinje cells and their dendritic arbors in the molecular layer (ml) (Sekerková et al., 2003). **B-B″**: Espin antibody does not label the peripheral processes of the SGNs, which connect to the intensely espin-positive inner hair cells (inner HC). **C-C″**: Espin antibody labels a large proportion of SGNs. Arrowheads point to examples of espin-negative, but TuJ1-positive type-I SGNs. **D-D″**: Spiral ganglion from a neighboring section showing no labeling when preimmune IgG (PI-IgG) is substituted for espin antibody. **E-E″**: Espin antibody does not label the vestibular ganglion (VG). Scale bars, A-A′, 200 μm; B-B′, 20 μm: C-E″, 50 μm. A magenta-green version of this figure can be viewed online as Supplementary Figure 1.

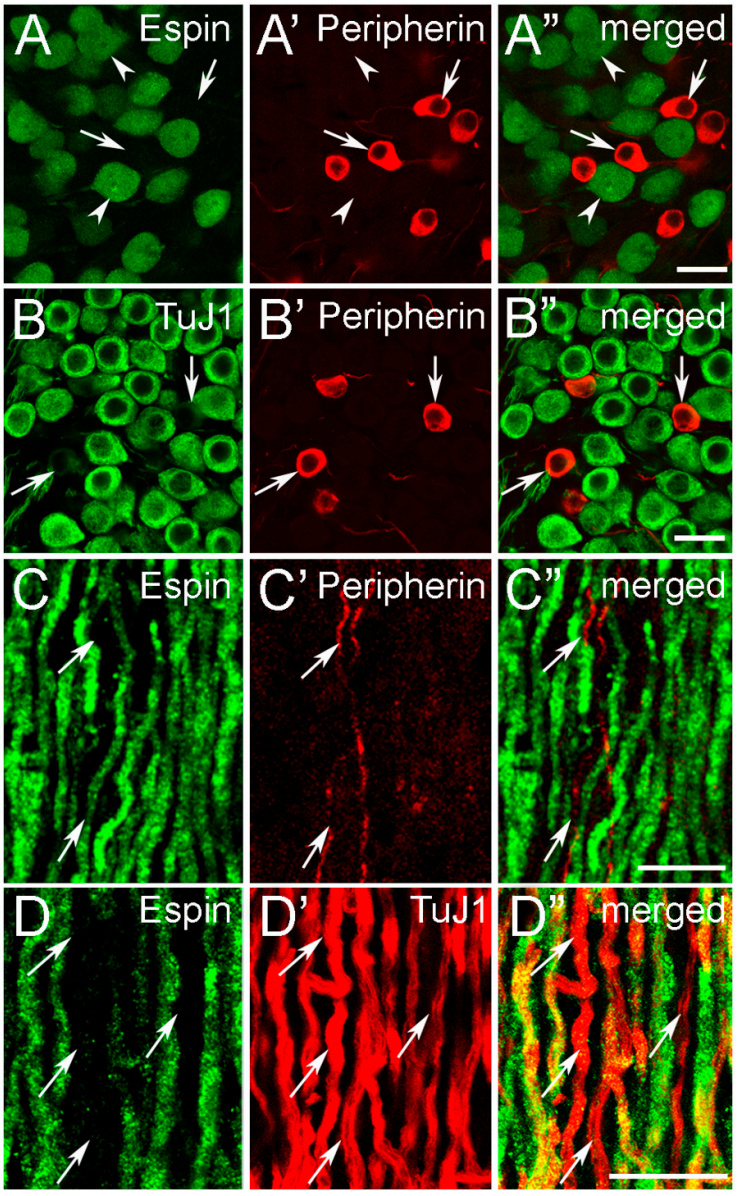

Fig. 2.

Confocal immunofluorescence localization of espins in type-I SGNs and their central fibers. Adult cochlea (decalcified) (A-B″) or CN cryosections (C-D″) labeled with the designated antibodies. **A-A″**: Espin antibody only labels the type-I SGNs (arrowheads). The peripherin-positive type-II SGNs are not labeled with espin antibody (arrows). **B-B″**: TuJ1 antibody preferentially labels the large, type-I SGNs, while the smaller type-II SGNs, which are labeled by peripherin antibody, show much weaker labeling with TuJ1 antibody (arrows). **C-C″**: In the auditory nerve, espins are present in the thick, type-I ANFs, but not in the thin, peripherin-positive type-II ANFs (arrows). **D-D″**: A large proportion of the large, intensely TuJ1-positive type-I ANFs is positive for espin. Arrows point to espin-negative type-I ANFs. Scale bars, 20 μm. A magenta-green version of this figure can be viewed online as Supplementary Figure 2.

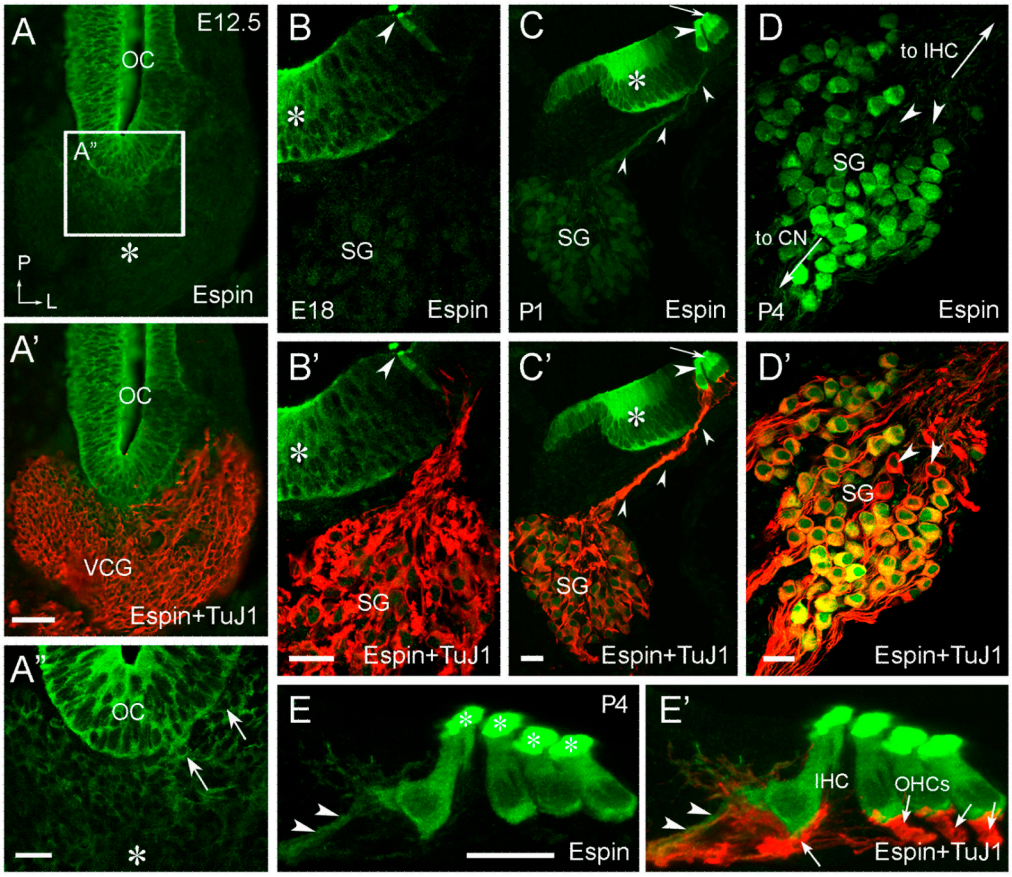

Fig. 3.

Immunofluorescence localization of espins in the developing inner ear. Cryosections labeled with espin antibody (green) and TuJ1 class III β-tubulin antibody (red). **A-A″**: In E12.5 embryos, intense espin antibody labeling is detected in the epithelial cells of the otocyst (OC). Delaminating espin-positive cells are observed near the anteroventral margin of the otocyst (arrows in A″). Cells in the body of the developing vestibulocochlear ganglion (VCG) show much lower levels of espin antibody labeling (asterisk). L, lateral; P, posterior. **B-B′**: In E18 embryos, the developing neurons of the spiral ganglion (SG) show extremely faint labeling in comparison to the espin-positive inner hair cell (arrowhead) and epithelial cells of the greater epithelial ridge (asterisk). **C-C′**: In P1 pups, the SGNs and their peripheral processes (small arrowheads) show faint espin antibody labeling. Espin antibody labeling is most intense in the outer (arrow) and inner (large arrowhead) hair cells, and it is still present at high levels in the otic epithelial cells that will go on to sculpt the inner sulcus (asterisk). **D-D′**: In P4 pups, espin antibody labels a large proportion of the SGNs. Arrowheads point to examples of espin-negative, TuJ1-positive SGNs. Large arrows show the direction of the peripheral fibers to inner hair cells (IHC) and ANFs to the CN. **E-E′**: A faint espin antibody labeling is detected in the SGN peripheral fibers (arrowheads), which appear to connect preferentially to the modiolar side of the inner hair cell (IHC) and not the outer hair cells (OHCs) (arrows in E′). Espin antibody labeling is especially intense in the sterocillia (asterisks) of the hair cells. Scale bars, A-A′, 50 μm; A″-E′, 20 μm. A magenta-green version of this figure can be viewed online as Supplementary Figure 3.

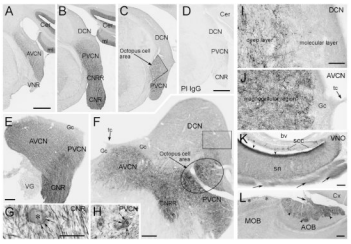

Fig. 4.

Immunoperoxidase localization of espins in the CN and vomeronasal nerve. **A-C:** Coronal brainstem cryosections show enrichment of espin antibody labeling in central nerve root (CNR) and central nerve root region (CNRR) (B), while distinct espin antibody labeling is also present in the AVCN (A), PVCN (B,C), the octopus cell area (C) and molecular layer (ml) of the cerebellum (Cer)(A,B). In these relatively low magnification images, the DCN does not appear to be labeled (B,C). Other structures of the brainstem, including the vestibular nerve root (VNR), are not labeled with espin antibody (A). **D:** No labeling is detected when the espin antibody is replaced with preimmune IgG. **E-F:** Parasagittal cryosections of CN illustrate espin antibody labeling in ANFs within the central nerve root (CNR) (E) and central nerve root region (CNRR) (F) and at their bifurcation to the AVCN and PVCN (E). Intense espin antibody labeling is also clearly discernible in the octopus cells area (F). Gc, espin-negative superficial granule cell layer and lamina; VG, espin-negative vestibular ganglion; tc, tenia choroidea. **G-H:** Higher magnification images showing a root neuron (asterisk in G) from the central nerve root (CNR) and octopus cells (asterisks in H) from the PVCN, which are apparent because they are surrounded by multiple espin-positive synaptic boutons (arrows). **I-J:** Higher magnification views of the DCN (from a similar region to that outlined by a box in F) and AVCN, showing espin-positive fibers and boutons in the deep layer and magnocellular layer, respectively. Note the absence of espin antibody-labeled fibers/boutons in the molecular layer and granule cell layer (Gc). **K:** In the vomeronasal organ (VNO), microvilli of the sensory neurons (sn) show the most intense labeling with espin antibody (arrowheads). The axons (arrows) of these cells are also labeled. bv, blood vessel; SCC, espin-positive solitary chemoreceptor cells (see Sekerková et al., 2004). **L:** In the accessory olfactory bulb (AOB), the nerve fibers (arrow) and the glomeruli (arrowheads) are distinctly labeled by espin antibody, while the neighboring glomeruli in the main olfactory bulb (MOB) appear espin-negative (asterisks). Cx, cortex. The sections in A-D,G,H are silver intensified to enhance the contrast of the DAB reaction product (see methods). Scale bars: A-D, 500 μm; E, F,L, 200 μm; G-K, 50 μm.

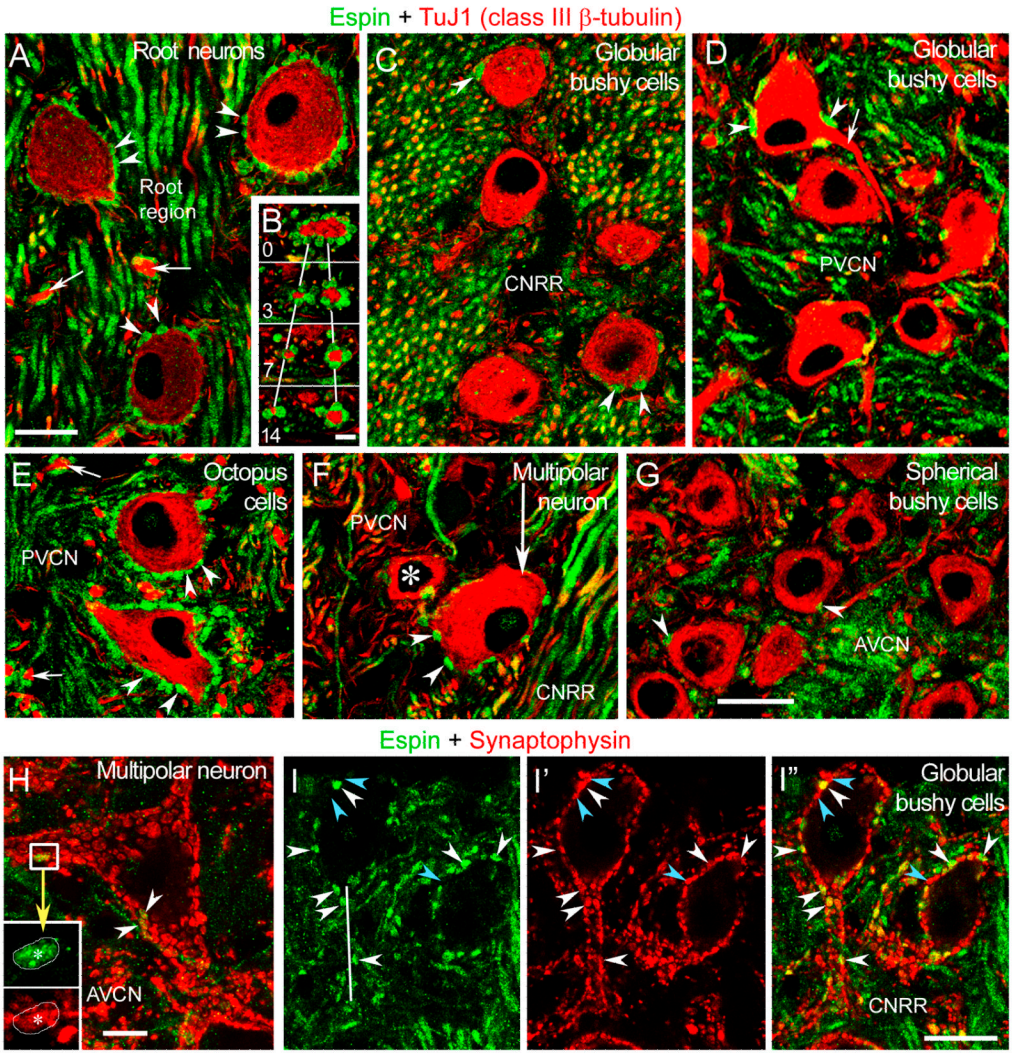

Fig. 5.

Confocal immunofluorescence images from various CN regions labeled with espin antibody (green) and either TuJ1 class III β-tubulin antibody (red) (A-G) or synaptophysin antibody (red) (H-I″). **A-G:** These panels illustrate the presence of espin in synaptic boutons (arrowheads in A-G) that contact a variety of cells and dendrites (B and arrows in A,D,E). B, images of an emerging dendrite surrounded by espin-positive boutons taken at 0, 3, 7, and 14 μm focusing intervals. Asterisk in F, globular bushy cell. CNRR, central nerve root region. **H:** A large multipolar neuron receives only a few espin-positive boutons (arrowheads and inset). This is a stack of 6 consecutive 1 μm thick confocal images. **I-I″**: Espins colocalize with synaptophysin in boutons contacting globular bushy cells (white arrowheads). This is a stack of 2 consecutive 1 μm thick confocal images. Blue arrowheads point to examples of espin-negative, synaptophysin-positive boutons. CNRR, central nerve root region. Scale bars: A, C-I″, 20 μm; and B, 5 μm. A magenta-green version ofthis figure can be viewed online as Supplementary Figure 4.

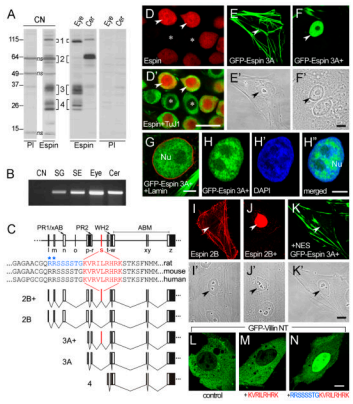

Fig. 6.

Espins in SGNs include splice-isoforms with a functional NLS. **A:** Western blots labeled with espin antibody (Espin) or preimmune IgG (PI) showing the presence of multiple specifically labeled bands in CN that correspond to the designated espin isoform size class (1 through 4) on the basis of apparent molecular mass and by comparison with known espin isoforms in other tissues. The CN sample is compared with samples of cerebellum (Cer) and eye, which were prepared from approximately one-half the wet tissue mass used for CN, on the same gel and western blot. The lanes are separated in the figure for clarity and to facilitate side-by-side comparisons with the corresponding lanes from the duplicate control western blot that was labeled with preimmune IgG. Bands labeled with espin antibody alone are bona fide espin bands, whereas those labeled with preimmune IgG and espin antibody are, by definition, nonspecific (ns). Note that the apparent abundance and/or apparent molecular masses of the nonspecific bands can differ from tissue to tissue. **B:** Ethidium bromide-labeled agarose gel analysis of the espin RT-PCR products obtained using primers in exons w and z (see C, below) showing the presence of espin transcripts in total RNA in isolated rat P4 spiral ganglion (SG). Also shown are the RT-PCR products obtained using comparable levels of total RNA prepared from P4 CN, eye, cerebellum (Cer) and the cochlear “sensory epithelium” (SE), which remained after removal of the spiral ganglion by micro-dissection and contains the hair cells. **C:** Exon maps of the espin gene (top) and selected espin isoforms (bottom, names at left) showing the position of the 27-nt exon s (red), which encodes the KVRILRHRK nonapeptide. The amino acids sequences of the nonapeptide (red) and surrounding sequences in rat, mouse and human espin isoforms are shown in the middle of panel C. The upstream octapeptide encoded by exon r, which also contributes to the bipartite NLS, is shown in blue. The two positively charged R residues in this peptide are marked by blue asterisks. PR1, proline-rich peptide 1; xAB, the additional F-actin-binding site; PR2, proline-rich peptide 2; WH2, WASP homology 2 (WH2) domain; ABM, 116-amino acid C-terminal actin-bundling module; l-z, exon designations. The shaded part of exon z represents the 3′-untranslated region. **D,D′**: Confocal immunofluorescence of spiral ganglion cryosection showing espin antibody labeling in the cytoplasm and nucleus (arrowheads) of the SGNs (D) and TuJ1 antibody labeling only in the SGN cytoplasm (D′). Asterisks, examples of large, TuJ1-positive, espin-negative SGNs. **E-K′**: Confocal fluorescence microscopy showing that GFP-tagged (F-H″) or untagged (J,J′) espin constructs containing the KVRILRHRK nonapeptide, designated with a “+”, show nuclear accumulation in transfected LLC-PK1 cells, whereas the corresponding isoforms lacking the KVRILRHRK nonapeptide (E,E′,I,I′) accumulate in coarse cytoplasmic actin bundles. Double labeling with lamin antibody (G) or DAPI (H-H″) shows that the nuclear GFP-espin 3A+ is internal to the nuclear lamina and concentrated in the interchromatin space, respectively. Nu in G,H″, nucleus. K,K′, Addition of a leucine-rich nuclear export signal (NES) to the GFP-espin 3A+ construct shifts its localization from the nucleus to the

cytoplasm. Arrowheads in E-F′ and I-K′, nucleus. **L-N:** Confocal fluorescence localization of the GFP-Villin NT construct without (L) or with the designated peptide inserts (M,N) showing that the 17-amino acid peptide RRSSSSTGKVRILRHRK is sufficient to cause nuclear accumulation of the GFP-villin NT construct (N), but the KVRILRHRK nonapeptide is not (M). Scale bars: D-D′, 20μm; E-F′ and I-N, 10 μm; G-H″, 5 μm. A magenta-green version of this figure can be viewed online as Supplementary Figure 5.